Successes and Challenges Associated with Solution Processing of Kesterite Cu_2ZnSnS_4 Solar Cells on Titanium Substrates

Zhengfei Wei[a], *Thomas O. Dunlop*[a], *Peter J. Heard*[b], *Cecile Charbonneau*[a], *David A. Worsley*[a] *and Trystan M. Watson**[a]

[a]*SPECIFIC, College of Engineering, Swansea University, Bay Campus, Swansea, SA1 8EN, Wales, U.K.*

[b]*Interface Analysis Centre, School of Physics, University of Bristol, Tyndall Avenue, Bristol, BS8 1TL, U.K.*

*) Corresponding Authors: Zhengfei.Wei@swansea.ac.uk and T.M.Watson@swansea.ac.uk

KEYWORDS: CZTS, titanium, solar cell, stress, SIMS

ABSTRACT: Roll-to-roll (R2R) processing of solution-based $Cu2ZnSn(S,Se)_4$ (CZT(S,Se)) solar cells on flexible metal foil is an attractive way to achieve cost-effective manufacturing of photovoltaics. In this work we report the first successful fabrication of solution-processed CZTS devices on a variety of titanium substrates with up to 2.88% power conversion efficiency

(PCE) collected on flexible 75 µm Ti foil. A comparative study of device performance and properties is presented aiming to address key processing challenges. First, we show that a rapid transfer of heat through the titanium substrates is responsible for the accelerated crystallisation of kesterite films characterised with small grain size, a high density of grain boundaries and numerous pore sites near the Mo/CZTS interface which affect charge transport and enhance recombination in devices. Following this, we demonstrate the occurrence of metal ion diffusion induced by the high temperature treatment required for the sulfurization of the CZTS stack: Ti^{4+} ions are observed to migrate upwards to the Mo/CZTS interface whilst Cu^{1+} and Zn^{2+} ions diffuse through the Mo layer into the Ti substrate. Finally, residual stress data confirm the good adhesion of stacked materials throughout the sequential solution process. These findings are evidenced by combining electron imaging observations, elemental depth profiles generated by secondary ion mass spectrometry, and x-ray residual stress analysis of the Ti substrate.

INTRODUCTION

Recent advances in thin film compound semiconductor photovoltaics have demonstrated much of the high potential of these technologies for generating sustainable and cost-efficient energy. Both $Cu(In,Ga)Se_2$(CIGS) and CdTe have achieved power conversion

efficiencies (PCEs) above 20% and they are well developed industrially.[1] Emerging light absorbing materials such as $Cu_2ZnSn(S,Se)_4$ (CZT(S,Se)) only contain earth abundant elements, providing more sustainable alternative to 2nd generation PV technologies. A number of research teams have now successfully fabricated over 10% efficiency CZT(S,Se) solar cell devices at the laboratory scale[2-4], encouraging further development aiming towards higher economic impact.[5-6] To address manufacturing costs, light-weight flexible materials such as metal or polymer foils can be used as substrates in roll-to-roll manufacturing. The high power-to-mass ratio of flexible solar cells favours their use in sectors such as building integrated photovoltaics (BIPV), aerospace and automotive power generation, and powering Internet of Things (IoT). Recent advances have been made in the vacuum fabrication of CZT(S,Se) solar cells produced on flexible substrates. For instance, CZT(S,Se) light absorbers were successfully grown directly on stainless steel foil to make photovoltaic devices reaching just over 6% efficiency.[7-8] Other metallic substrates such as molybdenum foil[9-10] and flexible glass[11] have been tested with PCEs reaching up to 6.78% and 3.09%, respectively. In comparison, the performance of devices fabricated with solution processed absorbers remains much lower than their vacuum counterpart with cell efficiencies of 1.94% reported on aluminium foil-based

devices[12], 4.4%[13] and 2.42%[14] on molybdenum foil, and 0.49% on polyimide[15].

Whilst most metal foils appear suitable for roll-to-roll manufacturing of PV devices owing to their flexibility and high electrical conductivity, other parameters need to be considered when optimising the manufacturing CZTS devices. For instance, it is desirable that the substrate is characterised with good chemical stability and has durable mechanical properties. In addition, the behaviour of the metal foil at high temperature (required for the preparation of the CZTS film) is also of great importance. In this work, we report the first successful preparation of solution-processed CZTS solar cells on titanium flexible (thickness: 50 µm and 75 µm) and rigid (thickness: 500 µm and 1000 µm) substrates (shown in **Figure 1**) and compare their performance to devices built on 1 mm soda-lime glass. A two-step stack-building process was applied where the active layer was spin-coated from a liquid precursor and sulphurisation carried out according to a procedure described in previous work.[16-17] Cross sectional electron microscopy observations, secondary ion mass spectrometer analysis (SIMS), and residual stress analysis of the Ti substrates were applied to understand the performance trends in CZTS devices.

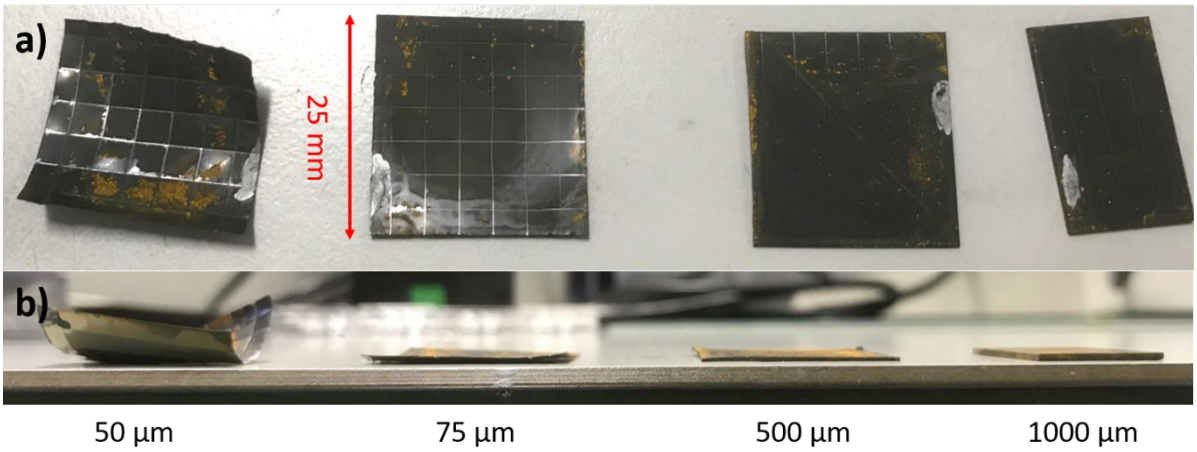

Figure 1. Flexible and rigid CZTS solar cells fabricated on 50-1000 µm Ti substrates: a) top view; b) side view.

EXPERIMENTAL SECTION

1) Substrates and cleaning procedure

Four types of Ti substrates were investigated which thickness (50 µm, 75 µm, 500 µm and 1000 µm), Ti content 99.6-99.9% w.t., and processing have been summarised in **Table S1**, together with those of the control soda-lime glass substrate. Cleaning was operated in an ultrasonic bath sequentially using soap water, deionised water, acetone, and isopropanol. Oxygen plasma treatment followed to remove any residual surface contaminants.

2) Preparation of Mo, CZTS layers, and top contacts

A 400 nm-thick molybdenum (Mo) film was deposited at room temperature by direct current (DC) magnetron sputtering using Kurt Lesker PVD 75 system. The C-Z-T-S precursor solutions were prepared by dissolving $CuCl_2 \cdot 2H_2O$ (98% Alfa Aesar), $SnCl_2$ (98% Sigma-Aldrich), $ZnCl_2$ (99.95% Alfa Aesar) and thiourea $SC(NH_2)_2$ (99% Sigma-Aldrich) in 5mL DMSO (99.9% Sigma-Aldrich). The $CuCl_2 \cdot 2H_2O$

concentration was 0.55 M and the targeted molar ratio of $SnCl_2$:$ZnCl_2$: $CuCl_2 \cdot 2H_2O$:thiourea was 1.31:0.69:1:1.84. All the precursor solution was doped with 0.14M NaCl. After the back contact deposition, the CZTS layers were grown on Mo/Ti substrates by spin-coating of the C-Z-T-S solution precursors. Samples were subsequently sulphurised in a rapid thermal processing furnace (RTP, MTI Corporation) at 560 °C for 20 mins. The thickness of the CZTS absorbers was 1.0-1.5 µm. After coating CZTS layers, a ~70 nm thick CdS layer was deposited by chemical bath deposition. ZnO (~75nm) and Al:ZnO (~500 nm) were radio frequency (RF) sputtered with respective power density of 1.87 Wcm^{-2} and 2.46 Wcm^{-2} served as a transparent top contact using a Moorfield Nanolab 60 sputtering system. The transmittance and reflectance of AZO film were shown in **Figure S1**. The single cells (0.4 cm x 0.4 cm = 0.16 cm^2) were defined by manual mechanical scribing.

3) Characterisation of materials and devices

Residual stress measurements were carried out with a Bruker D8 Discover X-ray diffraction system with a 0.07° step size, at a time of 7 s per step. The undertaken scans covered the full 0–0.9 $\sin2(\psi)$ in both positive and negative ψ tilts to confirm the absence of shear stress. Peak evaluation was undertaken using the Pearson VII fitting and stresses were calculated using a biaxial stress model, assuming $\sigma_{33}=0$.

CZTS/Mo/Ti samples were cross-sectioned using an FEI Helios NanoLab 600 combined focused ion beam/scanning electron microscope. Initially, protective platinum deposits of 20 µm x 2.5 µm x 1 µm thickness were made within the instrument using gas-assisted deposition in the presence of a platinum-bearing organometallic gas, in conjunction with a gallium focused ion beam. Vertical trenches (20 µm length x 10 µm width x 10 µm depth) were cut into the materials stack using a gallium focused ion beam of 30 keV energy and 20 nA beam. The vertical face of the section was then cleaned with the gallium ion beam at a reduced current of 6.5nA to produce high-quality surfaces enabling electron microscopy observations.

High magnification (x 25,000) images of the vertical sections were acquired using a JEOL-JSM-7800F field emission scanning electron microscope in secondary electron mode (10 keV beam energy and 0.34 nA beam current, 10 mm WD).

Secondary ion mass spectrometry (SIMS) depth profiles were obtained using an instrument built by the Interface Analysis Centre, at the University of Bristol. This system is featured with an electronically variable aperture type gallium ion gun (FEI SD gallium LMIS EVA focusing column) fitted to a double focusing magnetic sector mass analyser (Vacuum Generators model 7035). The experimental details can be found in our previous report[17]. Signals for sodium, titanium, copper, zinc, molybdenum and tin were

collected with dwell times of 1s per element, cycling through the elements for a total period of 30 minutes.

Current–density–voltage (*J–V*) curves were measured under simulated AM1.5G spectrum and 100 mW/cm^2 (1 sun) illumination. The external quantum efficiency (EQE) measurements were performed in AC mode with a chopping frequency of 67 Hz using a QEX10 system (PV Measurements) calibrated with a NIST-certified Si photodiode.

RESULTS AND DISCUSSION

1) Device performance

Substrate characteristics including thermal expansion properties, surface roughness, substrate composition and processing condition are critical elements to enable manufacturing of CZTS solar cells on flexible metal substrates.[18-20] Here, we selected Ti as our substrate material rather than commonly used stainless steel foil (SS) due to the smaller mismatch of coefficient of thermal expansion (CTE) of Mo/Ti than Mo/SS [18, 21] and their chemically stability as thin Ti coatings (50-60 nm-thick) were introduced as a diffusion barrier on SS based device in a previous report[7, 22-23]. We choose rigid (thickness: 500 µm and 1000 µm) Ti substrate to give a direct comparison to SLG substrate. For most flexible (thickness: 50 µm) Ti substrate, there is no apparent deformation through the whole coating processes until the mechanical scribing. Some layer-stack were peeled off due to its softness and sensitive to pressure variation caused by mechanical

scribing. The 75 µm-thick Ti foil shows the best flexibility versus mechanical stability of fabricated final solar cell device.

The PCE, V_{OC}, J_{SC}, and *FF* of CZTS cells built on Ti and SLG substrates are compared in **Figure 2** and best-performing cells parameters summarised in **Table 1**. Overall, cells prepared on titanium substrates recorded encouraging outputs with average PCEs of 1.49%, 2.08%, 1.81%, and 1.02% for 50, 75, 500, and 1000 µm Ti-based cells. The highest Ti-based device performance of 2.88% was collected on 75 µm flexible titanium substrate. However, this was lower than control SLG-based devices characterised with average PCEs of 4.85 % and a maximum at 5.29%. The gap in performance between Ti-based and SLG-based devices was associated with an important difference in J_{SC} related to high levels of porosity (**Figure 3, 4 and S2**) linking with elements diffusion (**Figure 5**) and overall higher series resistances (R_s) of Ti-based devices, which may stem from the formation of highly resistive secondary phases such MoS_2[24] and Ti_2S[25] at the back contact as evidenced by XRD and SIMS (**Figure S3 A, B and Figure 5**). Raman spectra of CZTS films prepared on 50, 75, 500, and 1000 µm Ti substrates and on SLG (**Figure S3 C and D**) show almost no difference on the spectra of these samples, which means three samples have similar crystalline phases at CZTS film surface. An examination of samples cross sections (**Figure 3, 4** and **Figure S2**) revealed that CZTS films prepared over Ti substrates had similar thickness (~ 1-1.5 µm) but

smaller grain size (< 200 nm) compared to films produced on SLG (up to 700-800 nm). Smaller crystals and higher densities of grain boundaries have been shown to hinder charge transport across CZTS films[26-27] and are here responsible for decreased R_{SH}. The Ti-based films also displayed high levels of porosity compared to SLG-based films. The absence of active material in pore sites greatly affected the density of charges produced and impacted on average device J_{SC}. This was in good agreement with the EQE data which confirmed lower levels of charge generation across the entire wavelength range (Figure 2). Higher levels of charge recombination evidenced by lower R_{sh} data, J_{SC} and fill factor were assigned to the enhanced density of CZTS/void and CZTS/CZTS grain boundaries which are prone to defects and known to act as recombination sites.[27-28] Finally, the V_{OC} of Ti-based devices, ranging between 0.40-0.47 V, was also found to be systematically lower than the V_{OC} of SLG-based devices averaging 0.57 V. EQE data (**Figure 2**) demonstrated very little variations in the bandgap of CZTS films across all samples (1.547-1.575 eV for the Ti-based films compared to 1.562 eV for the SLG-based film). Hence, we suspect the difference in V_{OC} is attributed to the formation of a thicker MoS_2 layer [7] enabled by the effective conduction of heat through Ti substrates. This is evidenced by increased R_s which is caused by high resistivity of the thick MoS_2 layer[29] and XRD peaks at 26° and

32° in Ti-based devices as compared to SLG-based devices[24] (**Table S2 and Figure S3 A and B**).

A comparison of photovoltaic performance for Ti-based devices only showed little effect of the substrate thickness. However, devices built over 50 µm and 1000 µm Ti substrates were characterised with lower average PCEs of 1.49 % and 1.02% compared to 2.08 % and 1.81 % for devices built over 75 µm and 500 µm Ti substrates. In the case of devices prepared on Ti-1000 µm, lower average FF and R_{sh} were assigned to localized delamination between the Mo and Ti layers in areas characterised with higher interface roughness, as illustrated in **Figure 3e**. The lower performance of devices prepared on 50 µm Ti substrates was attributed to the mechanical failure of the CZTS stack near mechanically scribed cell edges. The local deformation of the substrate, evidenced by the formation of ridges apparent at the top edge of the sample in **Figure 1a**, is thought to be responsible for the loss of CZTS material which translated into lower average J_{SC}. The other samples, built on far less flexible Ti substrates, remained unaffected by this process.

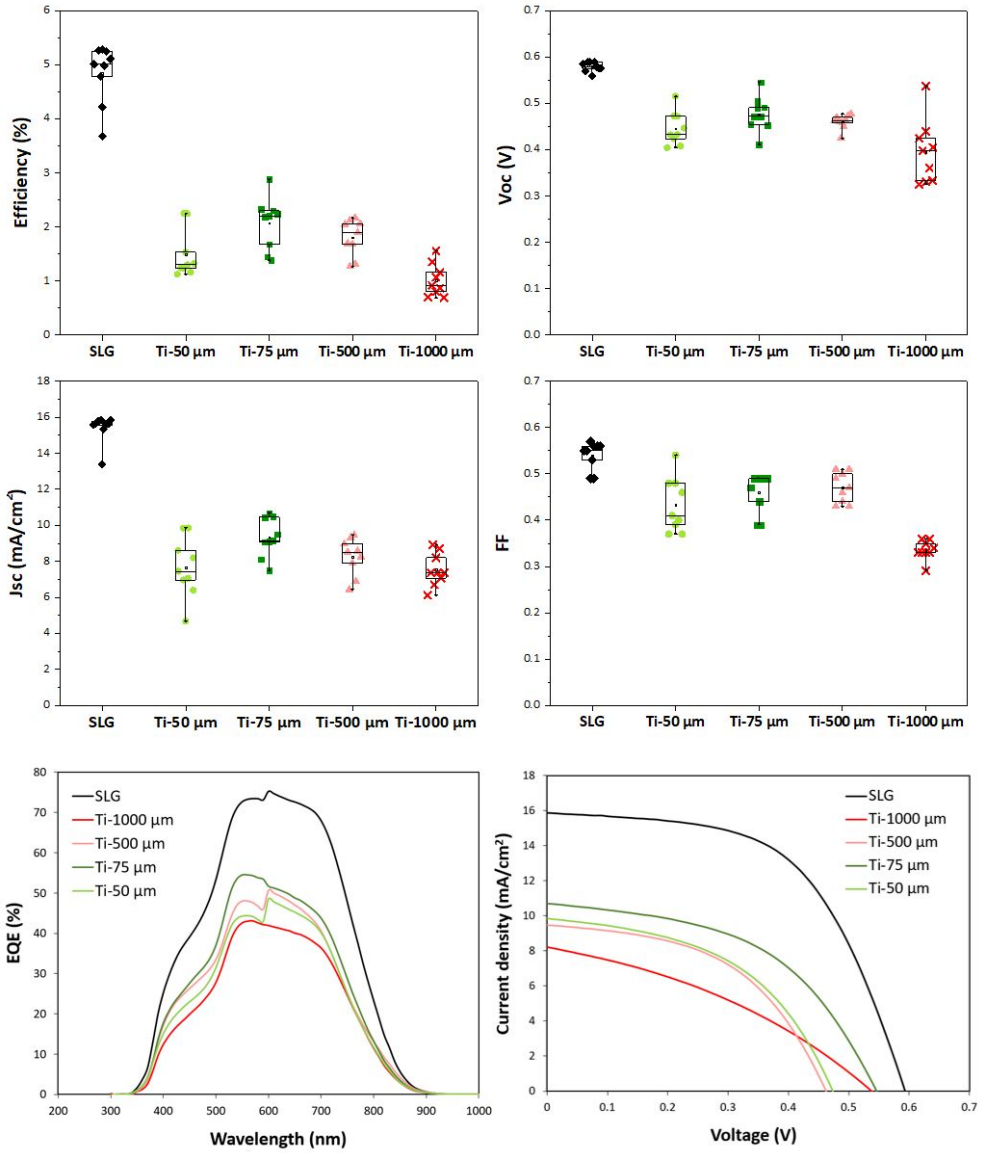

Figure 2. Box plots of J-V characteristics for CZT(S,Se) devices prepared on soda-lime glass (SLG) and 50, 75, 500, and 1000 µm Ti substrates.

Table 1. Summary of device parameters for the average values and the best-performing values of CZTS solar cells fabricated on 50, 75, 500, and 1000 µm Ti substrates and SLG.

Substrate	η (%)		V_{OC} (V)		J_{SC} (mA.cm^{-2})		FF	
Glass (SLG)	4.84±0.55	5.29	0.58±0.01	0.59	15.41±0.78	15.87	0.54±0.03	0.56
Ti-50 µm	1.49±0.45	2.25	0.45±0.04	0.47	7.67±1.67	9.85	0.43±0.06	0.48
Ti-75 µm	2.08±0.48	2.88	0.48±0.04	0.55	9.34±1.08	10.69	0.46±0.04	0.49
Ti-500 µm	1.81±0.34	2.17	0.46±0.02	0.46	8.25±1.03	9.45	0.47±0.03	0.50
Ti-1000µm	1.02±0.30	1.56	0.40±0.07	0.54	7.54±0.92	8.20	0.34±0.02	0.35

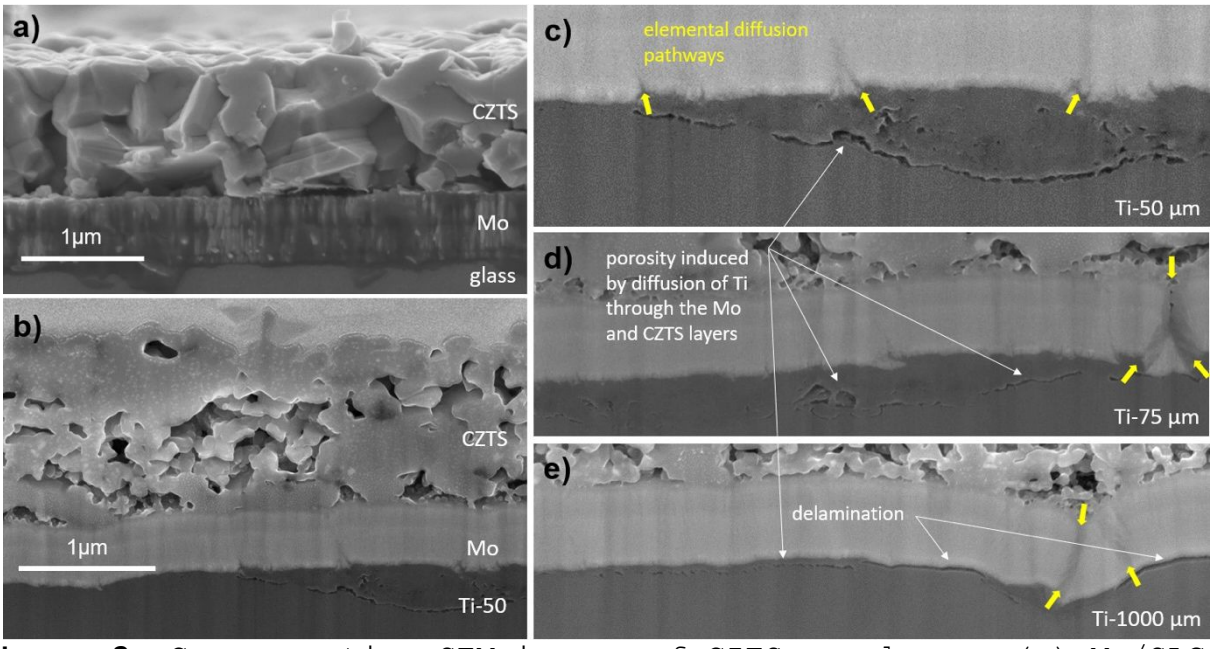

Figure 3. Cross-section SEM images of CZTS samples on (a) Mo/SLG-1000 µm; (b) Mo/Ti-50 µm. Selected areas of CZTS devices prepared on Ti substrates highlighting Ti diffusion pathways, residual Ti-

porosity and areas of delamination: (c) Mo/Ti-50 µm; (d) Mo/Ti-75 µm; (e) Mo/Ti-1000 µm.

2) Manufacturing challenges for Ti-based CZTS devices

Controlling the crystallisation of the CZTS layer to achieve large grains is critical to obtain efficient charge transport and optimum device performance.[26, 28] Various deposition methods have been developed to address these processing challenges.[7-9] In the case of solution processed films, it was demonstrated that is particularly important to tailor the heat treatment applied during this fabrication stage.[9] Here, a CZTS precursor containing metal chloride salts was spin coated onto Mo/Ti substrates and sulphurised in a rapid thermal processing furnace at 560 °C for 20 mins. Despite the great care taken in optimizing this process for SLG-based devices[16-17] results here show that further work is needed to achieve similar CZTS films on Ti substrates. As previously mentioned, a comparison of CZTS film cross-sections **Figure 3a** and **Figure 3b** showed overall much smaller crystals in Ti-based samples compared to SLG-based samples. A systematic assessment of crystal size across samples showed that all Ti-based samples were characterised with smaller CZTS crystals near the Mo/CZTS interface compared to the top part of the film. This has been evidenced in **Figure 4** where coloured areas highlight the occurrence of < 100 nm size crystals at the bottom of the films (in blue) and

over > 150 nm crystals (in red) at the centre and top parts of the films. An increasing crystal size upwards through the CZTS film suggests a gradient in the nucleation rate. This was not the case of SLG-based CZTS film where the size distribution of crystals was much larger and consistent across the thickness of the film. Titanium is known to conduct heat a lot more effectively than glass with a thermal conduction coefficient of 24 W/m·K, almost 25 times higher than soda lime glass ranging between 0.7-1.3 W/m·K. Here, we can conclude that the temperature of Ti substrates raised faster than that of the SLG substrate, causing an acceleration of nucleation events at the bottom of the films. In terms of manufacturing, there may be an opportunity to develop low heat conduction layers allowing a finer control over CZTS crystallization. Alternately, the heat treatment applied to sulphurize the CZTS film should be optimized based on the nature of the substrate. Whilst the temperature profile of the sulphurization process may be adjusted, it may be of interest to investigate the application of selective heating techniques such as demonstrated for the crystallisation of perovskite light absorbers.[30]

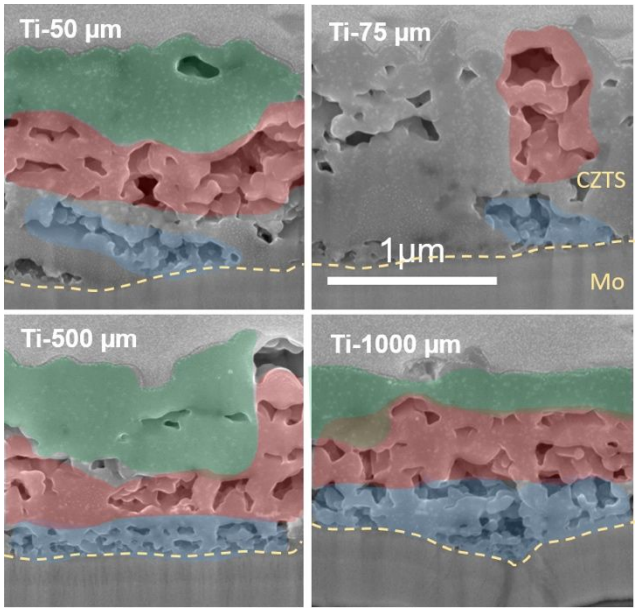

Figure 4. FEG-SEM cross sectional views of CZTS films built over Ti substrates highlighting areas characterised with small CZTS crystals (blue), large CZTS crystals (red), low levels of porosity (green).

Another challenge for the manufacturing of efficient metal-based CZTS devices is the diffusion of elements across layers of materials. The sulfurization of the molybdenum layer, an unwanted side effect of the high temperature sulphurization process, is already well documented.[17, 29, 31] But there are fewer published accounts addressing the diffusion of other elements, namely metallic ions.[7-8, 22] Sun *et al.* reported on the use of a Ti barrier layer aiming to prevent the diffusion of substrate Fe ions to the CZTS film.[7] To confirm the suitability of Ti with this regard, we investigated the motion of Ti ions of Ti-based CZTS stacks by combining cross-section imaging observations and secondary ion

mass spectrometry elemental depth profiling. At high magnification, the examination of the Mo/Ti interface (**Figure 5.a-d**) revealed the presence of pores in the Ti layer near the interface. Directly above these in the Mo layer, darker linear contrasts indicative of lower atomic weight elements was observed, sometimes extending across the entire thickness of the Mo layer. These strongly suggested the diffusion of Ti ions upwards areas, causing the formation of pores at the top of the Ti layer. These features were particularly pronounced in Ti-50 µm and Ti-75 µm stacks where heat conduction was more effective than in much thicker Ti-500 µm and Ti-1000 µm. This hypothesis was further confirmed by SIMS depth profile data. **Figure 6** shows elemental signals collected for Cu, Sn, Zn, Ti, Mo, and Na plotted against the etching time. All samples exhibited common features: 1) between 0-250 s etching time, high levels of Cu, Zn, and Sn were recorded which were assigned to the CZTS layer; 2) between 250-550 s etching time, decreasing levels of Cu, Zn, and Sn but high levels of Na and Mo suggested a transition to the Na-doped Mo layer; 3) over 550s etching time, the Ti signal became predominant as the etching gun reached the top of the metallic substrate. Similar elemental profiles had been collected for a SLG-Mo-CZTS stack in previous work.[17] However, in thin Ti-50 and Ti-75 µm substrates, a peak in Ti signal intensity was observed at approximately 300s, suggesting the accumulation of Ti atoms near the CZTS/Mo interface. This

confirms the diffusion of Ti across the Mo layer for these two samples (**Figure 3c** and **Figure 3d**). The same Ti peak was absent from depth profiles of samples built over thick Ti-500 and Ti-1000 µm substrates for which heat transfer was too slow to cause as significant diffusion of Ti (**Figure 5c** and **Figure 5d**). Another important finding relates to Cu and Zn elemental signals increasing after 500s of etching time, indicative the high concentrations of these elements at the Mo/Ti interface and in the depth of the Ti substrate. Increased Cu and Zn signals over 550s likely stems from oxygen enhancement effects (so called SIMS matrix effects) by formation of TiO_2 between the Mo layer and Ti substrate.[32-34] This suggests the occurrence of an inverse diffusion phenomenon where the upwards movement of Ti^{4+} ions was compensated by downwards migrations of Cu^{1+} and Zn^{2+} ions, possibly through the same pathways (**Figure 5b & 5c**). The diffusion of Cu and Zn also correlate higher densities of pores observed at the bottom of the CZTS film (**Figure 4 -** blue areas) compared to the top of the films generally characterised with lower levels of porosity (**Figure 4 -** green areas).

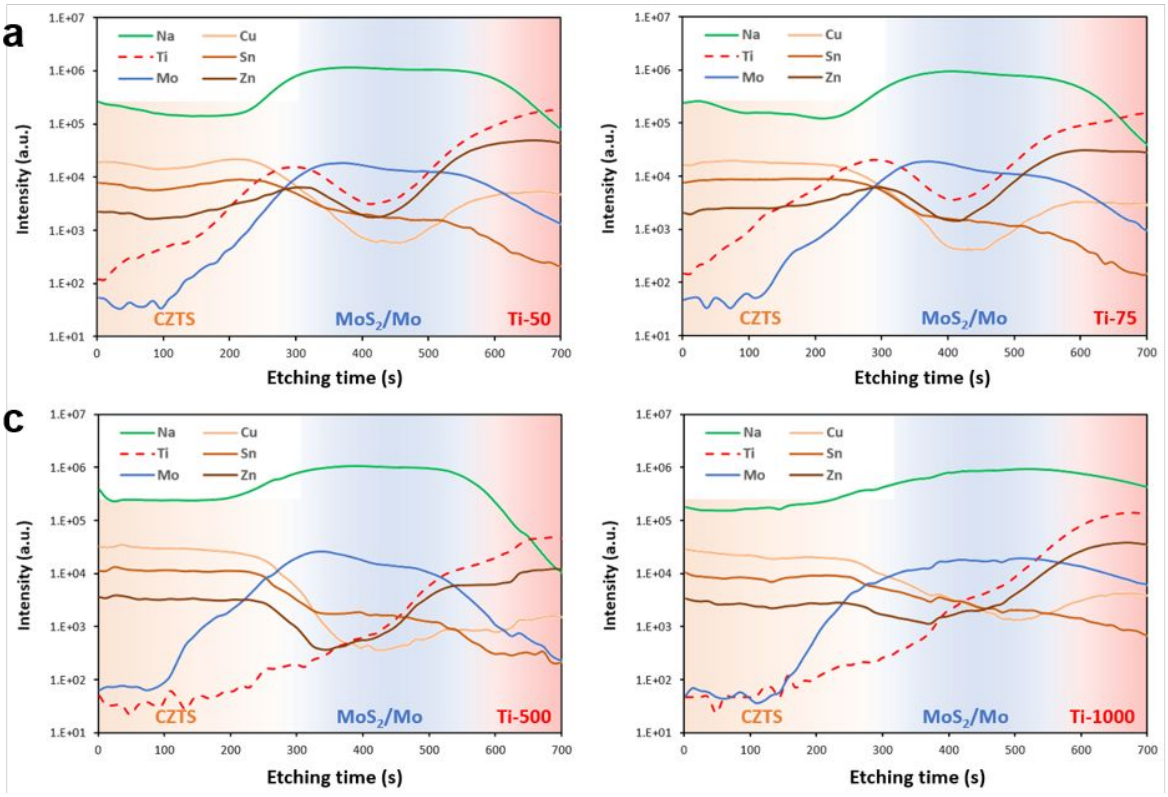

Figure 5. SIMS elemental depth profiles of CZTS samples on Ti substrates: (a) Mo/Ti-50 µm; (b) Mo/Ti-75 µm; (c) Mo/Ti-500 µm; (d) Mo/Ti-1000 µm CZTS, MoS_2/Mo and Ti are shown with orange, blue and red backgrounds, respectively.

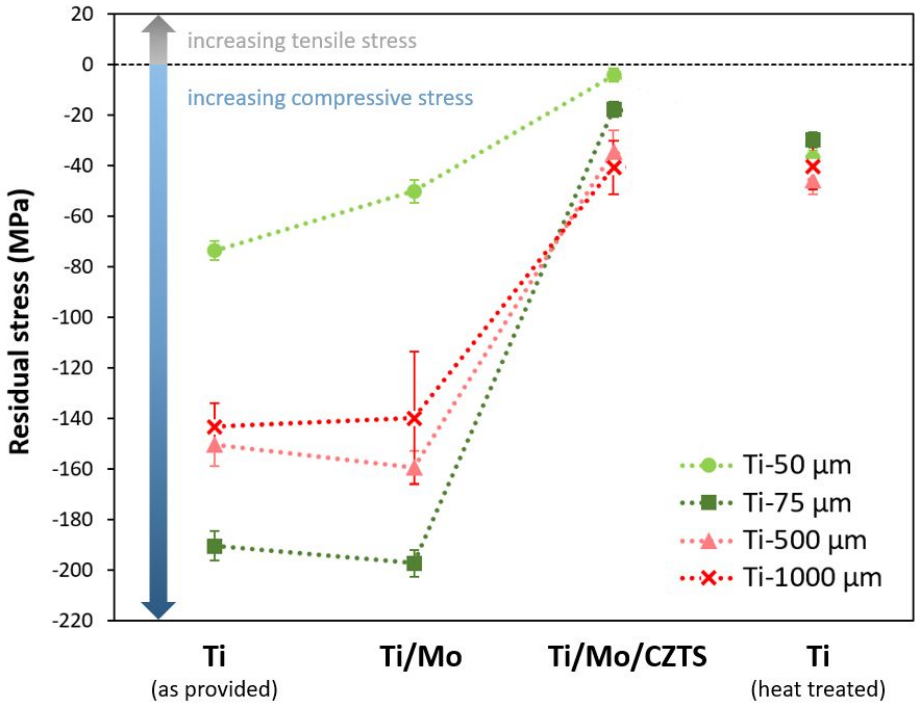

Figure 6. Residual stress analysis of Ti substrates in the σ_{11} direction using a biaxial model, following the application of a Mo layer (Mo/Ti), after the deposition and sulphurisation of the CZTS layer at 560 °C for 20 mins (CZTS/Mo/Ti), and for bare Ti substrates heated at 560 °C for 20min.

The mechanical stability of stacked layers of materials plays an important role in ensuring a successful transfer of photovoltaic technologies from lab scale to large roll-to-roll manufacturing. In previous work[17], we demonstrated that the sequential deposition of thin layers of Si_xN_y over Mo could induce compressive stress inside the Mo layer later on responsible for the delamination of the CZTS layer. In this work, the mechanical stability of our stacked layers was assessed by collecting x-ray residual stress

(σ_{11} and σ_{22} directions) data generated at the surface of the Ti layer, at each stage of the stack building process. Results presented in **Figure 6** indicate that all Ti substrates initially held compressive stresses of varying magnitude induced by the rolling of Ti bulk material into sheets and foils; this is despite the annealing treatment provided at the end of the manufacturing process which usually aims to release some of these stresses by promoting the re-organisation of the metallic crystalline matrix at high temperature. The data collected for Ti/Mo samples show that the deposition of a 400 nm Mo layer, operated at ambient temperature, had little effect over surface stress for most samples except for the Ti-50 µm samples which compressive stress decreased by 26% from -76.4±2.6 MPa to -58.1±4.2 MPa. However, the deposition and sulphurisation of the CZTS layer operated at 560 °C for 20 mins drastically reduced surface compressive stress in all Ti substrates. In particular, flexible Ti/Mo/CZTS samples with built on Ti-50 µm and Ti-75 µm displayed > 90 % loss whilst rigid samples built on Ti-500 µm and Ti-1000 µm displayed close to 75 % loss in surface compressive stress compared to their initial (Ti, as provided) state. The difference in stress release experienced by flexible compared to rigid Ti substrates may be assigned to faster temperature rise of the surface in the thinner substrates. The relaxation of Ti substrates throughout the stack building steps correlates the good mechanical adhesion observed between the Ti

and Mo layers in all samples. Hence, localised short ranged delamination features observed at the Ti/Mo interface of the Ti-1000 µm sample (**Figure 3e**) are mostly assigned to locally high roughness. Further testing was carried out on Ti substrates taken at 560 °C for 20 mins in the absence of other materials to confirm the impact of heat over the relaxation of Ti. As expected, we found that compressive stress was drastically reduced in heat-treated samples. However, it was not reduced as much as in Ti substrates of Ti/Mo/CZTS samples. This suggests that in the stack of materials, the re-organisation of Ti atoms at the surface of the Ti substrate was more efficient, supported by the bi-directional diffusion of metallic ions, namely Ti^{4+}, Cu^{1+}, and Zn^{2+} ions.

CONCLUSIONS

With this work we demonstrated the successful solution processing of CZTS solar cells on flexible Ti substrate with up to 2.88% power conversion efficiency achieve on 75 µm thick foil. Whilst this was achieved on a metal substrate readily usable for roll-to-roll manufacturing, specific issues related materials processing were highlighted. The unexpectedly efficient conduction of heat through the Ti substrate (compared to a sodium lime glass substrate, even at comparable thickness) led to the fast nucleation of CZTS crystals at the bottom of the layer, favouring the formation of small crystals and pores which are detrimental to device efficiency. The top of the films crystalized much slower and

displayed larger crystals together with lower levels of porosity. Another undesirable phenomenon related to the diffusion of metallic ions: we observed the diffusion of Ti^{4+} ions from the substrate to the bottom part of the CZTS film whilst Cu^{1+} and Zn^{2+} leached out of the film and diffused downwards to the metallic substrate, contributing to further porosity. However, this may be prevented by introducing barrier layers, a method already successfully reported to minimize the conversion of Mo to MoS_2.[17] In terms of device characteristics, increased recombination and resistance losses were found in the bulk of the CZTS film prepared on Ti substrates compared to SLG-based devices. These were associated with thermally induced porosity and high density of grain boundaries, pronounced MoS_2 formation and metallic ions diffusion. These results suggest that further optimization of the sulfurisation process is necessary and may result in the fabrication of devices with outputs comparable to SLG-based devices.

ASSOCIATED CONTENT

Supporting Information Available: Characteristics of substrates, Transmittance and reflectance of AZO film, SEM images and photovoltaic performance parameters of the CZTS devices fabricated with different Ti substrate thicknesses are presented. This

material is available free of charge via the Internet at http://pubs.acs.org.

ORCID:

Zhengfei Wei: 0000-0002-4358-9287

Thomas O. Dunlop: 0000-0002-5851-8713

Peter J. Heard: 0000-0002-8926-4680

Cecile Charbonneau: 0000-0001-9887-2007

David A. Worsley: 0000-0002-9956-6228

Trystan M. Watson: 0000-0002-8015-1436

ACKNOWLEDGMENTS

The IMPACT operation has been part-funded by the European Regional Development Fund through the Welsh Government and Swansea University. The authors would like to thank the financial support provided by Engineering and Physical Sciences Research Council (EPSRC) through the SPECIFIC Innovation and Knowledge Centre Phase 2 (EP/ N020863/1) and Photovoltaic Technology based on Earth Abundant Materials – PVTEAM project (EP/L017792/1). We would like to acknowledge the assistance provided by Swansea University College of Engineering AIM Facility, which was funded in part by the EPSRC (EP/M028267/1), the European Regional Development Fund through the Welsh Government (80708) and the Ser Solar project via Welsh Government.

REFERENCES

(1) Green, M. A.; Hishikawa, Y.; Dunlop, E. D.; Levi, D. H.; Hohl-Ebinger, J.; Ho-Baillie, A. W. Y. Solar cell efficiency tables (version 52). *Progress in Photovoltaics: Research and Applications* **2018**, *26* (7), 427-436, DOI: doi:10.1002/pip.3040.
(2) Wang, W.; Winkler, M. T.; Gunawan, O.; Gokmen, T.; Todorov, T. K.; Zhu, Y.; Mitzi, D. B. Device Characteristics of CZTSSe Thin-Film Solar Cells with 12.6% Efficiency. *Advanced Energy Materials* **2014**, *4* (7), n/a-n/a, DOI: 10.1002/aenm.201301465.
(3) Yan, C.; Huang, J.; Sun, K.; Johnston, S.; Zhang, Y.; Sun, H.; Pu, A.; He, M.; Liu, F.; Eder, K.; Yang, L.; Cairney, J. M.; Ekins-Daukes, N. J.; Hameiri, Z.; Stride, J. A.; Chen, S.; Green, M. A.; Hao, X. Cu2ZnSnS4 solar cells with over 10% power conversion efficiency enabled by heterojunction heat treatment. *Nature Energy* **2018**, *3* (9), 764-772, DOI: 10.1038/s41560-018-0206-0.
(4) Xin, H.; Vorpahl, S. M.; Collord, A. D.; Braly, I. L.; Uhl, A. R.; Krueger, B. W.; Ginger, D. S.; Hillhouse, H. W. Lithium-doping inverts the nanoscale electric field at the grain boundaries in Cu2ZnSn(S,Se)4 and increases photovoltaic efficiency. *Physical Chemistry Chemical Physics* **2015**, *17* (37), 23859-23866, DOI: 10.1039/C5CP04707B.
(5) Jäger-Waldau, A. Market Challenges for CZTS-Based Thin-Film Solar Cells. In *Copper Zinc Tin Sulfide-Based Thin-Film Solar Cells*; Ito, K., Ed.; John Wiley & Sons Ltd: 2015; pp 43-51.
(6) Eslamian, M. Inorganic and Organic Solution-Processed Thin Film Devices. *Nano-Micro Letters* **2016**, *9* (1), 3, DOI: 10.1007/s40820-016-0106-4.
(7) Sun, K.; Liu, F.; Huang, J.; Yan, C.; Song, N.; Sun, H.; Xue, C.; Zhang, Y.; Pu, A.; Shen, Y.; Stride, J. A.; Green, M.; Hao, X. Flexible kesterite Cu2ZnSnS4 solar cells with sodium-doped molybdenum back contacts on stainless steel substrates. *Solar Energy Materials and Solar Cells* **2018**, *182*, 14-20, DOI: https://doi.org/10.1016/j.solmat.2018.02.036.
(8) López-Marino, S.; Sánchez, Y.; Espíndola-Rodríguez, M.; Alcobé, X.; Xie, H.; Neuschitzer, M.; Becerril, I.; Giraldo, S.; Dimitrievska, M.; Placidi, M.; Fourdrinier, L.; Izquierdo-Roca, V.; Pérez-Rodríguez, A.; Saucedo, E. Alkali doping strategies for flexible and light-weight Cu2ZnSnSe4 solar cells. *Journal of Materials Chemistry A* **2016**, *4* (5), 1895-1907, DOI: 10.1039/C5TA09640E.
(9) Yan, Q.; Cheng, S.; Li, H.; Yu, X.; Fu, J.; Tian, Q.; Jia, H.; Wu, S. High flexible Cu2ZnSn(S,Se)4 solar cells by green solution-process. *Solar Energy* **2019**, *177*, 508-516, DOI: https://doi.org/10.1016/j.solener.2018.11.030.

(10) Jo, E.; Gang, M. G.; Shim, H.; Suryawanshi, M. P.; Ghorpade, U. V.; Kim, J. H. 8% Efficiency Cu2ZnSn(S,Se)4 (CZTSSe) Thin Film Solar Cells on Flexible and Lightweight Molybdenum Foil Substrates. *ACS Applied Materials & Interfaces* **2019**, DOI: 10.1021/acsami.9b03195.
(11) Peng, C.-Y.; Dhakal, T. P.; Garner, S.; Cimo, P.; Lu, S.; Westgate, C. R. Fabrication of Cu2ZnSnS4 solar cell on a flexible glass substrate. *Thin Solid Films* **2014**, *562*, 574-577, DOI: https://doi.org/10.1016/j.tsf.2014.03.054.
(12) Tian, Q.; Xu, X.; Han, L.; Tang, M.; Zou, R.; Chen, Z.; Yu, M.; Yang, J.; Hu, J. Hydrophilic Cu2ZnSnS4 nanocrystals for printing flexible, low-cost and environmentally friendly solar cells. *CrystEngComm* **2012**, *14* (11), 3847-3850, DOI: 10.1039/C2CE06552E.
(13) Xu, X.; Qu, Y.; Campbell, S.; Le Garrec, M.; Ford, B.; Barrioz, V.; Zoppi, G.; Beattie, N. S. Solution processing route to Na incorporation in CZTSSe nanoparticle ink solar cells on foil substrate. *Journal of Materials Science: Materials in Electronics* **2019**, *30* (8), 7883-7889, DOI: 10.1007/s10854-019-01108-3.
(14) Sun, K.; Su, Z.; Yan, C.; Liu, F.; Cui, H.; Jiang, L.; Shen, Y.; Hao, X.; Liu, Y. Flexible Cu2ZnSnS4 solar cells based on successive ionic layer adsorption and reaction method. *RSC Advances* **2014**, *4* (34), 17703-17708, DOI: 10.1039/C3RA47823H.
(15) Zhou, Z.; Wang, Y.; Xu, D.; Zhang, Y. Fabrication of Cu2ZnSnS4 screen printed layers for solar cells. *Solar Energy Materials and Solar Cells* **2010**, *94* (12), 2042-2045, DOI: https://doi.org/10.1016/j.solmat.2010.06.010.
(16) Wei, Z.; Zhu, M.; McGettrick, J. D.; Kissling, G. P.; Peter, L. M.; Watson, T. M. The effect of additional sulfur on solution-processed pure sulfide Cu2ZnSnS4 solar cell absorber layers. *MRS Advances* **2016**, *FirstView*, 1-6, DOI: doi:10.1557/adv.2016.425.
(17) Wei, Z.; Fung, C. M.; Pockett, A.; Dunlop, T. O.; McGettrick, J. D.; Heard, P. J.; Guy, O. J.; Carnie, M. J.; Sullivan, J. H.; Watson, T. M. Engineering of a Mo/SixNy Diffusion Barrier to Reduce the Formation of MoS2 in Cu2ZnSnS4 Thin Film Solar Cells. *ACS Applied Energy Materials* **2018**, *1* (6), 2749-2757, DOI: 10.1021/acsaem.8b00401.
(18) Kessler, F.; Rudmann, D. Technological aspects of flexible CIGS solar cells and modules. *Solar Energy* **2004**, 77 (6), 685-695, DOI: https://doi.org/10.1016/j.solener.2004.04.010.
(19) Zhang, Y.; Ye, Q.; Liu, J.; Chen, H.; He, X.; Liao, C.; Han, J.; Wang, H.; Mei, J.; Lau, W. Earth-abundant and low-cost CZTS solar cell on flexible molybdenum foil. *RSC Advances* **2014**, *4* (45), 23666-23669, DOI: 10.1039/C4RA02064B.

(20) Brémaud, D.; Rudmann, D.; Kaelin, M.; Ernits, K.; Bilger, G.; Döbeli, M.; Zogg, H.; Tiwari, A. N. Flexible Cu(In,Ga)Se2 on Al foils and the effects of Al during chemical bath deposition. *Thin Solid Films* **2007**, *515* (15), 5857-5861, DOI: https://doi.org/10.1016/j.tsf.2006.12.152.
(21) Yazici, S.; Olgar, M. A.; Akca, F. G.; Cantas, A.; Kurt, M.; Aygun, G.; Tarhan, E.; Yanmaz, E.; Ozyuzer, L. Growth of Cu2ZnSnS4 absorber layer on flexible metallic substrates for thin film solar cell applications. *Thin Solid Films* **2015**, *589*, 563-573, DOI: https://doi.org/10.1016/j.tsf.2015.06.028.
(22) Blösch, P.; Pianezzi, F.; Chirilă, A.; Rossbach, P.; Nishiwaki, S.; Buecheler, S.; Tiwari, A. N. Diffusion barrier properties of molybdenum back contacts for Cu(In,Ga)Se2 solar cells on stainless steel foils. *Journal of Applied Physics* **2013**, *113* (5), 054506, DOI: 10.1063/1.4789616.
(23) Buldu, D. G.; Cantas, A.; Turkoglu, F.; Akca, F. G.; Meric, E.; Ozdemir, M.; Tarhan, E.; Ozyuzer, L.; Aygun, G. Influence of sulfurization temperature on Cu2ZnSnS4 absorber layer on flexible titanium substrates for thin film solar cells. *Physica Scripta* **2018**, *93* (2), 024002, DOI: 10.1088/1402-4896/aa95eb.
(24) Olgar, M. A.; Tomakin, M.; Kucukomeroglu, T.; Bacaksız, E. Growth of Cu2ZnSnS4 (CZTS) thin films using short sulfurization periods. *Materials Research Express* **2019**, *6* (5), 056401, DOI: 10.1088/2053-1591/aaff78.
(25) Owens, J. P.; Conrad, B. R.; Franzen, N. F. The crystal structure of Ti2S. *Acta Crystallographica* **1967**, *23* (1), 77-82, DOI: 10.1107/s0365110x67002154.
(26) Wei, Z. Process development and optimisation for efficient and cost-effective Cu(In,Ga)Se2 thin film solar cells. PhD PhD thesis, Heriot-Watt University Edinburgh, 2014.
(27) Sardashti, K.; Haight, R.; Gokmen, T.; Wang, W.; Chang, L.-Y.; Mitzi, D. B.; Kummel, A. C. Impact of Nanoscale Elemental Distribution in High-Performance Kesterite Solar Cells. *Advanced Energy Materials* **2015**, *5* (10), 1402180, DOI: 10.1002/aenm.201402180.
(28) Bourdais, S.; Choné, C.; Delatouche, B.; Jacob, A.; Larramona, G.; Moisan, C.; Lafond, A.; Donatini, F.; Rey, G.; Siebentritt, S.; Walsh, A.; Dennler, G. Is the Cu/Zn Disorder the Main Culprit for the Voltage Deficit in Kesterite Solar Cells? *Advanced Energy Materials* **2016**, n/a-n/a, DOI: 10.1002/aenm.201502276.
(29) Scragg, J. J.; Wätjen, J. T.; Edoff, M.; Ericson, T.; Kubart, T.; Platzer-Björkman, C. A Detrimental Reaction at the Molybdenum Back Contact in Cu2ZnSn(S,Se)4 Thin-Film Solar Cells. *Journal of the American Chemical Society* **2012**, *134* (47), 19330-19333, DOI: 10.1021/ja308862n.

(30) Troughton, J.; Carnie, M. J.; Davies, M. L.; Charbonneau, C.; Jewell, E. H.; Worsley, D. A.; Watson, T. M. Photonic flash-annealing of lead halide perovskite solar cells in 1 ms. *Journal of Materials Chemistry A* **2016**, *4* (9), 3471-3476, DOI: 10.1039/C5TA09431C.
(31) Scragg, J. J.; Kubart, T.; Wätjen, J. T.; Ericson, T.; Linnarsson, M. K.; Platzer-Björkman, C. Effects of Back Contact Instability on Cu2ZnSnS4 Devices and Processes. *Chemistry of Materials* **2013**, *25* (15), 3162-3171, DOI: 10.1021/cm4015223.
(32) Yu, M. L. Chemical enhancement effects in SIMS analysis. *Nuclear Instruments and Methods in Physics Research Section B: Beam Interactions with Materials and Atoms* **1986**, *15* (1), 151-158, DOI: https://doi.org/10.1016/0168-583X(86)90273-9.
(33) Vickerman, J. C. Secondary ion mass spectrometry-basic concepts, instrumental aspects, applications and trends. A. BENNINGHOVEN, F. G. RUDENAUER and H. W. WERNER, Wiley, New York, 1987, 1277 pages. *Surface and Interface Analysis* **1987**, *10* (8), 435-435, DOI: 10.1002/sia.740100811.
(34) Oueslati, S.; Brammertz, G.; Buffière, M.; ElAnzeery, H.; Mangin, D.; ElDaif, O.; Touayar, O.; Köble, C.; Meuris, M.; Poortmans, J. Study of alternative back contacts for thin film Cu2ZnSnSe4-based solar cells. *Journal of Physics D: Applied Physics* **2014**, *48* (3), 035103, DOI: 10.1088/0022-3727/48/3/035103.

Graphical abstract